PLOS ONE

RESEARCH ARTICLE

Quantification of pulsed electric field for the rupture of giant vesicles with various surface charges, cholesterols and osmotic pressures

Md. Kabir Ahamed, Marzuk Ahmed, Mohammad Abu Sayem Karal*

Department of Physics, Bangladesh University of Engineering and Technology, Dhaka, Bangladesh

* asayem221@phy.buet.ac.bd

OPEN ACCESS

Citation: Ahamed M.K, Ahmed M, Karal MAS (2022) Quantification of pulsed electric field for the rupture of giant vesicles with various surface charges, cholesterols and osmotic pressures. PLoS ONE 17(1): e0262555. https://doi.org/10.1371/journal.pone.0262555

Editor: Jian Xu, East China Normal University School of Life Sciences, CHINA

Received: October 1, 2021

Accepted: December 28, 2021

Published: January 13, 2022

Data Availability Statement: All relevant data are within the paper.

Funding: This study was supported by the Ministry of Science and Technology, Bangladesh (No. 39.00.0000.009.14.011.20-Phy's-566/1902), Ministry of Education, Bangladesh (No. 37.20.0000.004.033.020.2016.1053), Information and Communication Technology Division (ICTD), (Ministry of Posts, Telecommunications and Information Technology), Bangladesh (No. 56.00.0000.028.33.105.18-05) and Committee for

Abstract

Electropermeabilization is a promising phenomenon that occurs when pulsed electric field with high frequency is applied to cells/vesicles. We quantify the required values of pulsed electric fields for the rupture of cell-sized giant unilamellar vesicles (GUVs) which are prepared under various surface charges, cholesterol contents and osmotic pressures. The probability of rupture and the average time of rupture are evaluated under these conditions. The electric field changes from 500 to 410 Vcm^{-1} by varying the anionic lipid mole fraction from 0 to 0.60 for getting the maximum probability of rupture (i.e., 1.0). In contrast, the same probability of rupture is obtained for changing the electric field from 410 to 630 Vcm^{-1} by varying the cholesterol mole fraction in the membranes from 0 to 0.40. These results suggest that the required electric field for the rupture decreases with the increase of surface charge density but increases with the increase of cholesterol. We also quantify the electric field for the rupture of GUVs containing anionic mole fraction of 0.40 under various osmotic pressures. In the absence of osmotic pressure, the electric field for the rupture is obtained 430 Vcm^{-1}, whereas the field is 300 Vcm^{-1} in the presence of 17 $mOsmL^{-1}$, indicating the instability of GUVs at higher osmotic pressures. These investigations open an avenue of possibilities for finding the electric field dependent rupture of cell-like vesicles along with the insight of biophysical and biochemical processes.

1 Introduction

Biomembranes are selectively permeable barrier which separates the interior and exterior of an organism [1,2]. Various types of equivalent circuit of biomembranes are considered by different groups [3–5]. Large electric potential is rare in living organisms, except in the region of cell membrane which is about—70 mV [6]. This potential is crucial for the transport of ions either into the lumen or out from the cells [7,8]. Because of least invasive nature and flexibility to adjust the strength, the external electric field has long been recognized as an excellent external agent for disrupting the cells [9–11]. Synthetic lipid vesicles such as giant unilamellar vesicles (GUVs) are being used as an attractive tool in soft matter research for the mimicking of cells since a few decades [12,13]. Lipid membranes of GUVs are significantly affected by the

Advanced Studies and Research (CASR) of Bangladesh University of Engineering and Technology (BUET), Bangladesh (No. DAERS/R-01/CASR-339th/2021) to Mohammad Abu Sayem Karal. The funders had no role in study design, data collection and analysis, decision to publish, or preparation of the manuscript. There was no additional external funding received for this study.

Competing interests: The authors have declared that no competing interests exist.

external electric field due to the charges on their polar head groups and the limited permeability of the hydrophobic tail to the solvent. Considering the electrical environment of cells or vesicles, external electric field can interact with the lipid membranes in various ways by influencing electrical properties such as electrical conductivity [14,15], membrane capacitance [16,17], transmembrane voltage [18,19] etc. Several types of phenomena can occur depending on the nature of electric field, for example, permeabilization [20–22], fusion [23,24], electrophoresis [25] and deformation [26,27]. Among them, electroporation is a vastly accepted technique, responsible for the generation of pores in vesicles when they are subjected to large electric field that can promptly increase the permeability of membranes. Sufficiently high electric potential applied to the membrane promotes stretching instability, which leads to the pore formation since the applied electric field increases membrane bending stiffness and lowers membrane tension [28]. The process of electroporation is actually twofold [29]. Firstly, a molecular rearrangement of the lipid occurs within the membrane bilayer induced by electrostatic forces and secondly, the Maxwell stress tensor starts to rise from the applied electric field. There is an increase in membrane current and membrane dynamic conductance with the ascending transmembrane voltage [30]. Now-a-days, electroporation is commonly used in many areas of biomedical, biotechnology, bioengineering, and medicine, for applications such as cell fusion [31,32], electrochemotherapy [11,33,34], gene transfer [35,36], cancer treatment along with localized tumor ablation [34,37,38], food processing [39,40] and so on. Based on the electric field parameters, this permeabilization is either reversible or irreversible [41–43]. A limited number of studies on membrane permeabilization due to electric field have already been performed as an attempt to improve and model the effects of electric field parameters, such as intensity and duration [44–46]. In the molecular dynamic (MD) simulations, it is evident that the transmembrane voltage is generated either by a direct electric field or by charging of membranes [47,48]. Continuum-level description of membrane electroporation from MD simulations has been compared to the experimental measurements on model lipid systems [49,50]. There is a general consideration that transmembrane voltage, induced by electric field, promotes rupture of GUVs. So far, there is no cognizant report on the quantification of electric field for vesicle rupture under various conditions such as surface charges and cholesterol contents of the membranes, and osmotic pressures in the vesicles. Hence, the experimental measurements of the values of external electric fields and the average times for the rupture of GUVs under those conditions are indispensable.

2 Materials and methods

2.1 Chemicals and reagents

1,2-dioleoyl-*sn*-glycero-3-phospho-(1′-*rac*-glycerol) (sodium salt) (DOPG) and 1, 2-dioleoyl-*sn*-glycero-3-phosphocholine (DOPC) were purchased from Avanti Polar Lipids Inc. (Alabaster, AL). Bovine serum albumin (BSA), 1,4-Piperazinediethanesulfonic acid (PIPES), Ethylene glycol-bis(2-aminoethylether)-*N*,*N*,*N*′,*N*′-tetraacetic acid (EGTA) and calcein were purchased from Sigma-Aldrich (Germany). Cholesterol (i.e., Chol) was purchased from WAKO pharmaceuticals (Japan).

2.2 Preparation of GUVs at various conditions

The anionic charged GUVs were prepared in a physiological buffer (10 mM PIPES, 150 mM NaCl, pH 7.0, 1mM EGTA) and the neutral GUVs were prepared in MilliQ water using the natural swelling method [51]. Here, the method is described briefly. A mixture of 1 mM DOPG and DOPC (about 200 μL) or DOPG, DOPC and Chol were taken into a glass vial and dried with a gentle flow of N_2 gas for producing thin and homogeneous lipid films. By keeping

the vial in a vacuum desiccator for 12 hours, the residual chloroform in the film was removed. Then, 20 μL MilliQ water was added into the vial and pre-hydrated at 45–47˚C for 8 minutes. After pre-hydration, the sample was incubated with 1 mL of buffer containing 0.10 M sucrose for about 3 hours at 37˚C. To prepare water-soluble fluorescent probe (calcein) containing GUVs, vesicles were incubated in the buffer with 0.10 M sucrose containing 1 mM calcein. The incubated GUV suspension (unpurified) was centrifuged at ~ 13,000×g (here g is the acceleration due to gravity) for ~ 20 minutes at ~ 20˚C for removing the multilamellar vesicles and lipid aggregates as these elements were sedimented at the bottom of eppendorf tubes. After centrifugation, supernatant was collected and purified by the membrane filtering method [52,53].

To prepare the GUVs with different surface charges, the DOPG mole fractions (X_{DOPG}) were considered 0.60, 0.40, 0.20, 0.10, 0. Hence, the samples were DOPG/DOPC (60/40, here 60/40 indicates molar ratio), DOPG/DOPC (40/60), DOPG/DOPC (20/80), DOPG/DOPC (10/90) and DOPG/DOPC (0/100)-GUVs. To prepare cholesterol (Chol) containing membranes, the samples DOPG/DOPC/Chol (60/40/0), DOPG/DOPC/Chol (46/39/15), DOPG/DOPC/Chol (43/28/29) and DOPG/DOPC/Chol (40/20/40)-GUVs were prepared in the same buffer. The corresponding cholesterol mole fraction in these samples were 0, 0.15, 0.29 and 0.40. By considering the surface areas of DOPG and cholesterol [54–59], the surface charge density of these cholesterol containing membranes were obtained almost similar (~ - 0.15 Cm^{-2}). For performing the osmotic pressure experiments, DOPG/DOPC (40/60)-GUVs were prepared in the buffer under various osmotic pressures (Π). The osmolarity of the sucrose solution inside the GUVs was C^0_{in} = 388 $mOsmL^{-1}$, whereas the osmolarities of the glucose solution outside the GUVs were C_{out} = 388, 375 and 371 $mOsmL^{-1}$. Hence, the corresponding osmolarity difference between the inside and outside of GUVs were $\Delta C^0 = C^0_{in} - C_{out}$ = 0, 13 and 17 $mOsmL^{-1}$. Due to the osmolarity difference between sucrose and glucose solutions, vesicles became swell as water molecules of glucose solution passed into the inside of GUVs through membranes. The osmotic gradient creates lateral tension in the membranes of GUVs. The detail procedure to apply the Π in GUVs has been described in our recent paper [60]. To avoid the strong adhesion between the GUVs and the surface of glass slide, the chamber was coated with 0.10% (w/v) BSA dissolved in the same buffer.

2.3 Model to apply the electric field on vesicle using COMSOL simulation

To estimate the electric potential gradient and the distribution of current density on a vesicle, the finite element method-based software COMSOL Multiphysics was used. The simulation was used to investigate transport processes in various model systems [61]. The parameters of the model are summarized in Table 1. The electrodes were modeled as two rectangular plates placed at the left and right of the center of geometry. The mesh size was refined until there was less than 5% difference in electric field, resulting an extremely fine mesh setting. The total number of degrees of freedom solved in the model was 153669. The model describes electric field strength and current density in a spherical shaped vesicle. The dynamic finite-element model for efficient modelling of electric currents in electroporated tissue has been described elsewhere [62]. The time dependent electric current density equation is as follows:

$$J = (\lambda + \varepsilon_0 \varepsilon_r \frac{\partial}{\partial t})E + J_e \quad (1)$$

where, λ is an electrical conductivity of the system and J_e is the charge density, ε_0 is the permittivity of free space and ε_r is the relative permittivity. The electric field (E) is the gradient of electric potential (V), i.e., $E = -\nabla V$.

Table 1. The parameters, materials and values for COMSOL simulation.

Parameters	Materials	Symbol	Values
Vesicle	Radius	R	12 μm
Membrane	Thickness	h	~ 4 nm
Interior of vesicle	Conductivity	λ_{in}	1.45 Sm^{-1}
	Relative permittivity	ε_{in}	70
Exterior of vesicle	Conductivity	λ_{ex}	1.45 Sm^{-1}
	Relative permittivity	ε_{ex}	70
Membrane of vesicle	Conductivity	λ_{m}	3.0×10^{-7} Sm^{-1}
	Relative permittivity	ε_{m}	4.5
	Resistivity	ρ_{m}	3.3×10^{6} Ωm

https://doi.org/10.1371/journal.pone.0262555.t001

The time dependent electric current module was used in the simulation where the parallel gold electrodes were selected. The numerical model demonstrated the importance of contact and angle between GUV and electrodes. For a certain value of electric potential with current density, the transmembrane voltage shows its threshold value for the rupture of targeted GUV.

2.4 Setup for applying the pulsed electric field on GUVs

A MOSFET based IRE device was used for generating the pulsating DC (direct current) electric field with pulse width 200 μs and frequency 1.1 kHz. The detail circuit diagram was published in the earlier papers [22,63]. The photograph of IRE setup is shown in Fig 1(A). The IRE signal is applied to the GUV (GUV is kept in a U-shaped handmade microchamber) through gold coated electrodes of length 17.0 mm and width 2.54 mm (SH-17P-25.5, Hellotronics). The pulsed electric field, and the illustration of intact and ruptured vesicles under various conditions are shown in Fig 1(B).

2.5 Theoretical equations for applying pulsed electric field on GUVs

From the electrical point, transmembrane voltage (V_m) is defined as the difference between the values of the homogeneous electric potential on both sides of the membrane. In the presence of pulsed electric field to a vesicle, when V_m exceeds ~ 1.0 V, the structural rearrangement of the lipid bilayer occurs, creating permanent aqueous pathways or pores in the membranes. The induced Vm at each membrane point is defined as follows [64]:

$$V_m = f_m RE|\cos\theta|(1 - e^{-t/\tau_{charg}}) \tag{2}$$

where, R is the radius of vesicle, θ is the angle between the electric field and surface potential and τ_{charg} is the membrane charging time constant. The expression for f_m is defined as follows [64]:

$$f_m = \frac{3\,\sigma_{ex}[3\,h\,R^2\sigma_{in} + (3\,h^2R - h^3)(\sigma_m - \sigma_{in})]}{2R^2(\sigma_m + 2\sigma_{in})(\sigma_m + \frac{1}{2}\sigma_{in}) - 2(R-h)^3(\sigma_{ex} - \sigma_m)(\sigma_{in} - \sigma_m)} \tag{3}$$

where, the conductivity of membrane is σ_m, internal medium is σ_{in}, external environment is σ_{ex}, and h is the thickness of membrane. Assuming $\sigma_m = 0$ (plasma membrane, $\sigma_m = 3\times10^{-7}$ Sm^{-1}), then $f_m = 1.5$. Hence, Eq (3) is expressed as the first-order Schwan's equation:

$$V_m = 1.5RE|\cos\theta|(1 - e^{-t/\tau_{charg}}) \tag{4}$$

where, τ_{charg} is the membrane charging-time, which is ~ 96.80 ns [22] for membrane

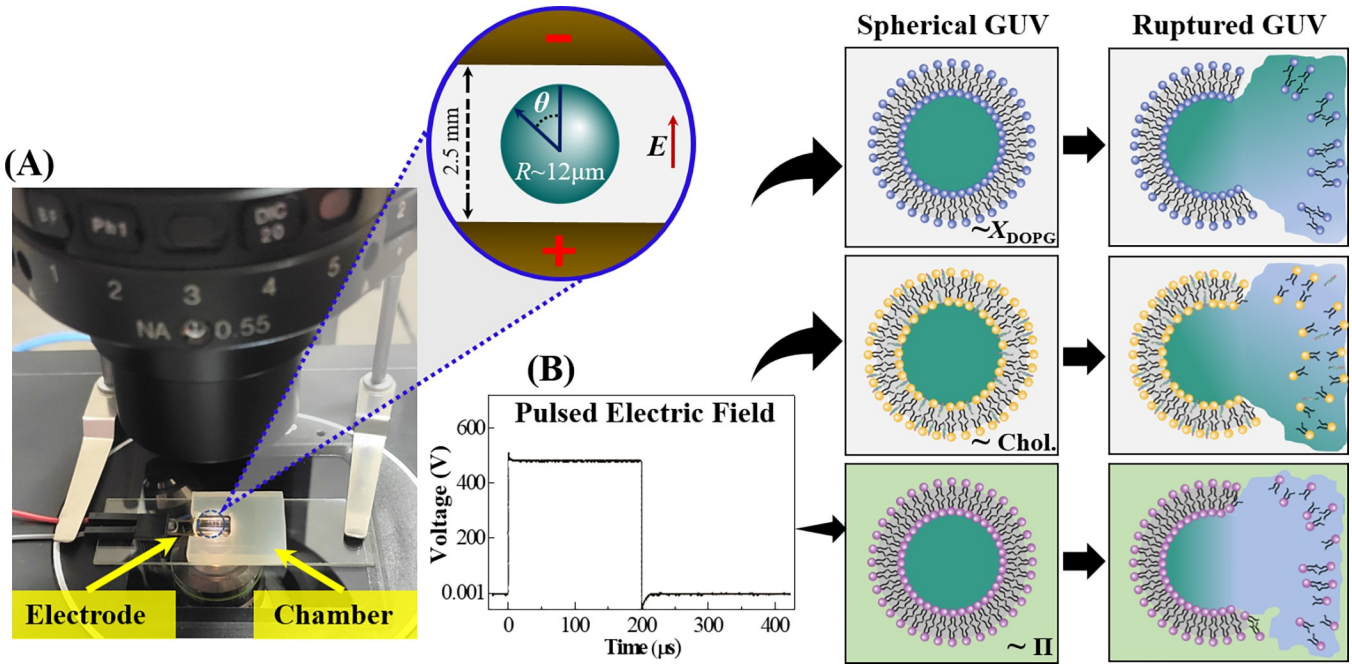

Fig 1. The electroporation processes. (A) Photograph of the electroporation setup with a scheme of a GUV between the electrodes (shown in the inset, not drawn to scale). (B) A pulsed electric field and the illustration of the electric field induced rupture of GUVs under DOPG lipid mole fraction (X_{DOPG}), cholesterol (Chol) content and osmotic pressure (Π).

https://doi.org/10.1371/journal.pone.0262555.g001

capacitance, $C_m \sim 1$ μFcm^{-1} and GUV radius $R = 10$ μm. Therefore, Eq (4) can be written as follows:

$$V_m = 1.5RE\cos\theta \tag{5}$$

The transmembrane voltage becomes maximum, when $\theta = 0$. The rupture of GUVs occurs in that membrane site where transmembrane potential has a maximum value. The maximum value of V_m (= V_c) is called the 'critical transmembrane voltage for breakdown' of vesicle. Then Eq (5) can be written as,

$$V_m = V_c = 1.5RE \tag{6}$$

The value of V_c depends on the values of R and E, and in this experiment V_c ranges from 0.60 to 1.17 V.

2.6 Observation technique combined with high speed imaging

To observe the dynamics of vesicles under external electric field, the GUVs were visualized by an inverted phase contrast fluorescence microscope (Olympus IX-73, Japan) with a 20× objective. All experiments were performed at 25 ± 1˚C. The images of GUVs were found from the recorded video using a charge-coupled device camera (Olympus DP22, Japan) with exposure time 111 ms. The frames per second (fps) of the camera was 25. A mercury lamp was used to acquire images of vesicles using the fast-digital camera. Phase contrast images were acquired using the cellSens Entry (Ver. 1.16) PC software (Olympus Corporation, Japan). The fluorescence intensity in the inside of GUVs was found from the active gray scale video using cellSens Dimension (Ver. 3.20) PC software (Olympus Corporation, Japan).

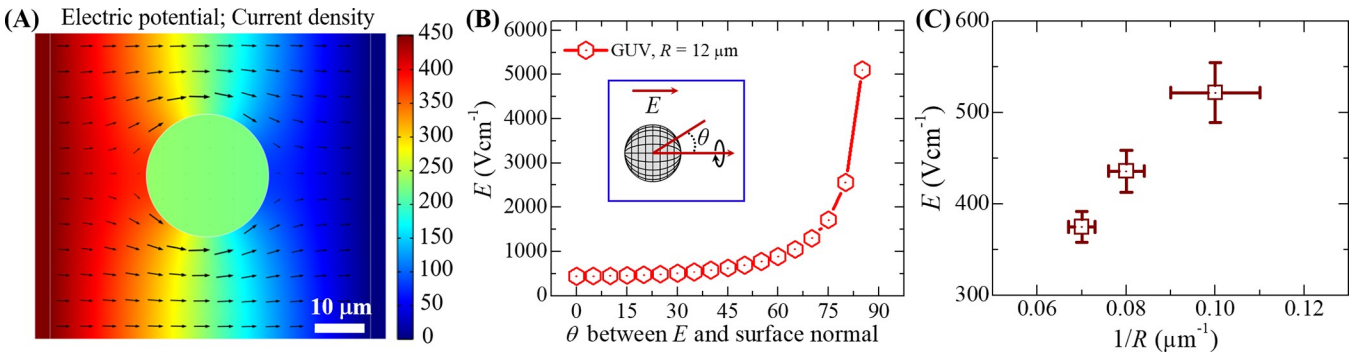

Fig 2. Electric field (*E*) strength for the permeabilization of spherical shaped GUV. (A) Distribution of current density with surface potential for lipid vesicle. The side color bar indicates the applied electric potential. (B) Electric field as a function of θ for R = 12 μm. (C) The 1/R dependent electric field for the rupture of GUVs.

https://doi.org/10.1371/journal.pone.0262555.g002

3 Results

3.1 Estimation of electric field for the rupture of GUVs using COMSOL simulation

Before going to quantify the electric field required for the rupture of vesicles, it was important to perform the simulation using the similar condition as used in the experimental study. It is mentioned earlier (see section 2.4) that the finite element-based software COMSOL Multiphysics is used to conduct the simulation. Fig 2(A) shows a simulation result in which the electric field was applied to a 'single GUV'. In this case, 450 V potential was applied to the left sided gold coated electrode while the right sided electrode acted as ground. It is to be noted that for a certain value of electric potential with current density, the transmembrane voltage must be given at its threshold value (V_c) for the rupture of GUVs. It was simulated the value of V_c for R = 12 μm GUV using Eq (6). The values of electric field with corresponding θ (θ is the angle between E and surface normal) is shown in Fig 2(B). It is very clear that the electric field required for the rupture of GUVs increases with the increase of θ. Moreover, all these values of E are responsible for rupturing of GUVs by creating pores in the membranes. If θ = 0, the rupture occurs at $E \sim 450$ Vcm^{-1}, while higher values of E are required for the rupture of GUVs if θ changes from 0 to 90˚. The value of electric field required for the rupture of GUVs is also dependent on the sizes of GUVs for a particular value of θ. As for example, E varied from 350 to 540 Vcm^{-1} for R = 10 to 15 μm at θ = 0. The 1/R dependent electric field required for vesicle rupture is shown in Fig 2(C) for the case of θ = 0. The value of E increases almost linearly with 1/R. This simulation work provided an important information on how much electric fields are needed for the rupture of GUVs in various experimental conditions.

3.2 Effect of pulsed electric field on the average time of rupture of GUVs

Here, the effect of pulsed electric field on a 'single GUV' has been investigated experimentally. In this case, an electric field, E = 390 Vcm^{-1} was applied on a 'single DOPG/DOPC (60/40)-GUV' (DOPG mole fraction X_{DOPG} = 0.60) for a maximum time 60 s. At time t = 0 s (i.e., before applying E due to electroporation signal), the GUV shows spherical structure in an inverted phase contrast image (Fig 3A(i)), and the structure remains unchanged until 10 s. The initiation of rupture starts at 11 s and subsequently the GUV is broken (Fig 3A(i)). Such rupture occurs due to the formation of pore in the membranes of vesicles as explained earlier [43,65]. The time of rupture is defined as the time when the vesicles start to rupture. We performed the similar experiment for 15–24 'single GUVs'. As for the presentation, we show only

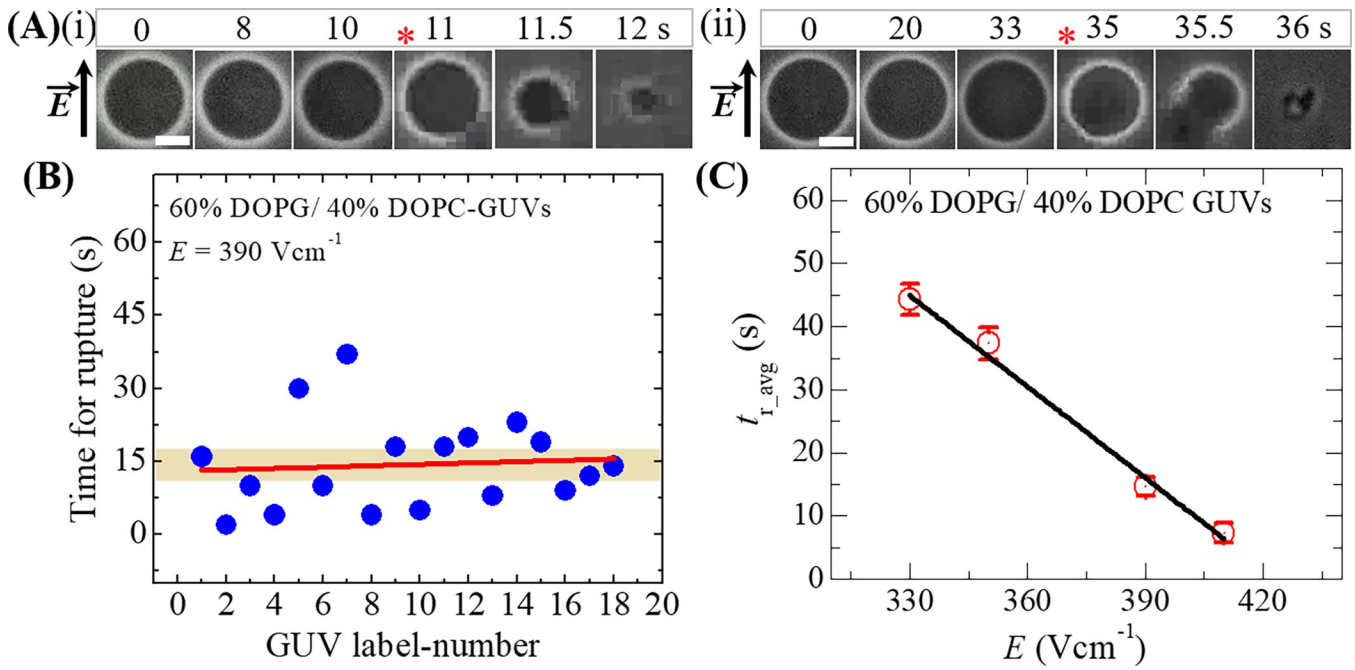

Fig 3. Stochastic rupture of several 'single GUVs' with phase contrast images and average rupture time after applying pulsed electric fields on the GUVs. (A) Phase contrast images of rupture of (i) first and (ii) second 'single DOPG/DOPC (60/40)-GUV' at $E = 390$ Vcm^{-1}. The field direction is shown with an arrow in the left side. The numbers above in each image indicate the time in seconds after application of electric field. The time of rupture is indicated by the asterisk (*). The white bar corresponds to a length of 10 μm. (B) The time of stochastic rupture in several single DOPG/DOPC (60/40)-GUVs (number = 18) at $E = 390$ Vcm^{-1}. (C) The E dependent average rupture time for DOPG/DOPC (60/40)-GUVs. The average values (t_{r_avg}) and standard deviations are obtained using 3 independent experiments, each with 15–24 GUVs for each E.

https://doi.org/10.1371/journal.pone.0262555.g003

two 'single' GUVs'. Fig 3A(ii) represents the rupture of the 2nd GUV, in which it occurs at 35 s. The rupture of several 'single GUVs' follows stochastic nature as shown in Fig 3(B), which means that the rupture of 18 GUVs occurs stochastically at different times in the presence of a fixed electric field (i.e., $E = 390$ Vcm^{-1}). We calculated the average time (t_{r_avg}) of the stochastic rupture by fitting the data. The solid red line (see Fig 3(B)) shows the linearly fitted curve from where $t_{r\_avg} = 14.4 \pm 4.7$ s is obtained. The similar experiment for rupture was done for $E = 330$, 350 and 410 Vcm^{-1} and calculated the t_{r_avg} in each condition. The value of t_{r_avg} decreases with the increase of E as shown in Fig 3(C). For $E = 330$ Vcm^{-1}, $t_{r\_avg} = 44.33 \pm 2.52$ s and for $E = 410$ Vcm^{-1}, $t_{r\_avg} = 7.33 \pm 1.53$ s.

The E dependent t_{r_avg} (s) data is fitted using a linear equation, and we obtain $t_{r\_avg} \sim 0$ s when $E \sim 420$ Vcm^{-1}. These investigations give us the information that how applied electric field influences the average time of the vesicle rupture. Interestingly, the values of external electric fields required for rupture of GUVs are very much consistent with the result as obtained in COMSOL simulation (see section 3.1).

3.3 Time of applied electric field dependent probability of rupture of GUVs

In this section, we experimentally investigated the probability of rupture (P_{rup_t}) until different times (t_{EF}) during the application of E. Fig 4 shows the dependence of P_{rup_t} of DOPG/DOPC (60/40)-GUVs for $E = 330$ Vcm^{-1} (■) until the time, $t_{EF} = 10$, 20, 40 and 60 s. The probability of rupture is defined as the number of ruptured GUVs divided by the total number of observed GUVs. Suppose a number of 20 GUVs are investigated in 20 individual microchamber till a particular time after applying a specific electric field. If 10 GUVs are ruptured, $P_{rup\_t} = 10/$

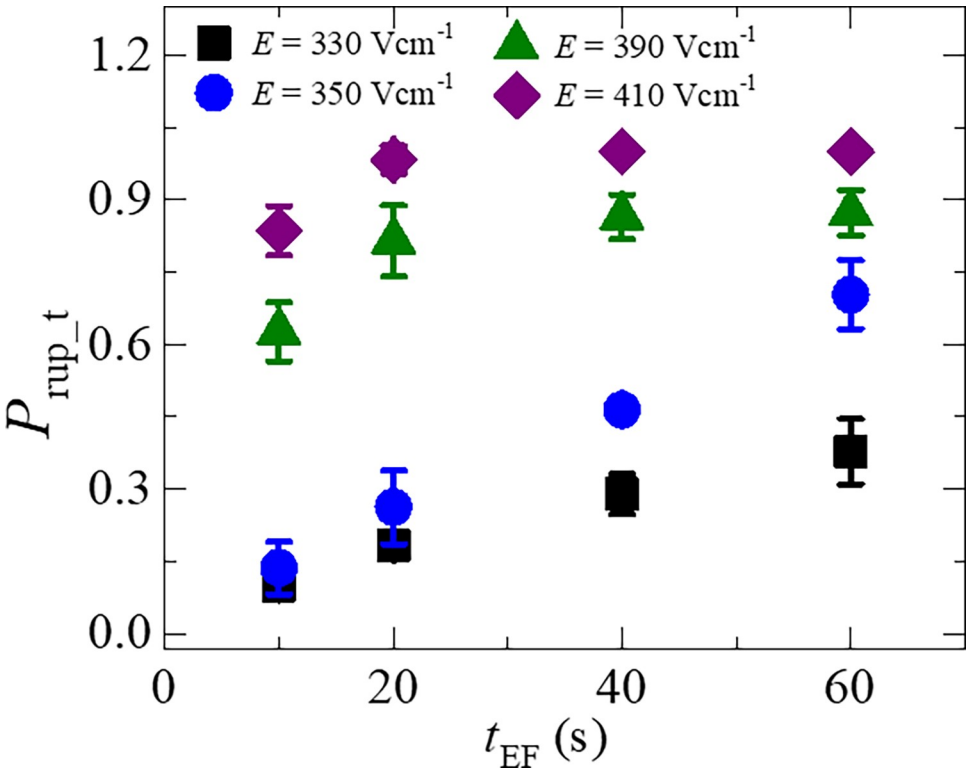

Fig 4. The time of applied electric field dependent probability of rupture of DOPG/DOPC (60/40)-GUVs until different time slots. Average and standard deviation are calculated from 3 independent experiments using 15–24 GUVs for each case.

https://doi.org/10.1371/journal.pone.0262555.g004

20 = 0.5. At first, we observe the results of $E = 330$ Vcm^{-1} in which the value of P_{rup_t} increases with the increase of t_{EF}. At 10 s, $P_{rup\_t} = 0.10 \pm 0.01$ and at 60 s, $P_{rup\_t} = 0.38 \pm 0.07$. Similar experiments were done for $E = 350$ Vcm^{-1} (●), $E = 390$ Vcm^{-1} (▲) and $E = 410$ Vcm^{-1} (◆) at the same time slot. In all conditions of electric field, the P_{rup_t} increases with t_{EF}.

However, at a particular time slot, the value of P_{rup_t} is higher for higher electric field. As for example, at $t_{EF} = 10$ s, $P_{rup\_t} = 0.14 \pm 0.05$ for $E = 350$ Vcm^{-1} and 0.86 ± 0.05 for $E = 410$ Vcm^{-1}. Moreover, at $E = 410$ Vcm^{-1}, $P_{rup\_t} = 1.0$ at 40 s and above. These investigations clearly show that the values of electric field required for rupture of GUVs are dependent on t_{EF}.

3.4 Quantity of electric field for the rupture of GUVs containing various surface charges

Here, we determine the electric field required for the rupture of GUVs prepared by various anionic charges in their membranes. The anionic charge was varied by changing the DOPG mole fraction (X_{DOPG}) at 162 mM salt concentration in buffer. Electric field $E = 420$ Vcm^{-1} was applied on DOPG/DOPC (40/60)-GUV (here $X_{DOPG} = 0.40$) for a maximum time 60 s. The phase contrast image of a spherical shaped GUV is shown in Fig 5A(i), which was intact until $t = 15$ s and then ruptured at $t = 15.5$ s. The same electric field was also applied on DOPG/DOPC (10/90)-GUV (here $X_{DOPG} = 0.10$) and rupture occurred at $t = 32.5$ s (Fig 5A (ii)). Fig 5(B) shows the dependence of probability of rupture until 60 s, P_{rup_60s}, for $X_{DOPG} =$ 0.60 (●), 0.40 (■), 0.20 (▼), 0.10 (⬢) and 0 (◆) for various E. In all cases of X_{DOPG}, the value of P_{rup_60s} increases with E. However, as the value of X_{DOPG} decreases from 0.60 to 0, the electric

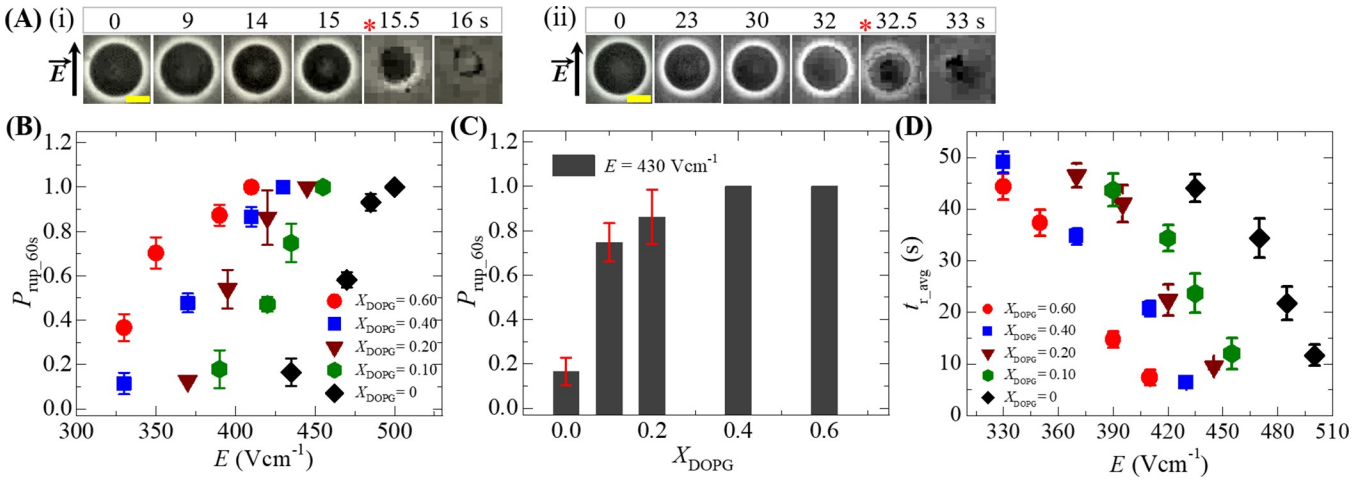

Fig 5. Electric field dependent probability of rupture and the average time of rupture of GUVs containing various surface charges in their membranes. (A) Phase contrast images of rupture of (i) a 'single DOPG/DOPC (40/60)-GUV' at $E = 420$ Vcm^{-1} and (ii) a 'single DOPG/DOPC (10/90)-GUV' at $E = 420$ Vcm^{-1}. The field direction is shown with an arrow in the left side. The numbers above in each image indicate the time in seconds after application of electric field. The time of rupture is indicated by the asterisk (*). The yellow bar corresponds to a length of 10 μm. (B) The electric field dependent P_{rup_60s} for X_{DOPG} = 0.60 (●), 0.40 (■), 0.20 (▼), 0.10 (⬢) and 0 (◆). (C) The X_{DOPG} dependent P_{rup_60s} at $E = 430$ Vcm^{-1}. (D) The electric field dependent average rupture time for X_{DOPG} = 0.60 (●), 0.40 (■), 0.20 (▼), 0.10 (⬢) and 0 (◆). Average and standard deviation are calculated from 3 independent experiments using 15–24 GUVs for each case.

https://doi.org/10.1371/journal.pone.0262555.g005

field required for the similar value of P_{rup_60s} is larger. As an example, $P_{rup\_60s} = 0.87 \pm 0.05$ for $X_{DOPG} = 0.60$ at $E = 390$ Vcm^{-1} whereas $P_{rup\_60s} = 0.86 \pm 0.12$ for $X_{DOPG} = 0.20$ at $E = 430$ Vcm^{-1}. It has also been investigated the X_{DOPG} dependence of P_{rup_60s} for a specific electric field. Fig 5(C) shows the P_{rup_60s} with X_{DOPG} for $E = 430$ Vcm^{-1} in which $P_{rup\_60s} = 0.16 \pm 0.06$ at $X_{DOPG} = 0$ is much lower than $P_{rup\_60s} = 0.86 \pm 0.12$ at $X_{DOPG} = 0.20$. The value of $P_{rup\_60s} = 1.0$ at $X_{DOPG} = 0.40$ and 0.60 for the same electric field.

In addition, we measured the average time of rupture (t_{r_avg}) for X_{DOPG} = 0.60 (●), 0.40 (■), 0.20 (▼), 0.10 (⬢) and 0 (◆) for various E as shown in Fig 5(D). The values of t_{r_avg} decrease with the increases of E for all X_{DOPG}. As an example, for $X_{DOPG} = 0.20$, $t_{r\_avg} = 49.00 \pm 2.00$ s at $E = 330$ Vcm^{-1}, $t_{r\_avg} = 34.67 \pm 1.53$ s at $E = 370$ Vcm^{-1}, $t_{r\_avg} = 20.67 \pm 1.53$ s at $E = 410$ Vcm^{-1} and $t_{r\_avg} = 6.33 \pm 0.58$ s at $E = 430$ Vcm^{-1}. Similar t_{r_avg} can be found by decreasing the electric fields for various X_{DOPG}. For better understanding, the value of $t_{r\_avg} = 34.67 \pm 1.53$ s at $E = 370$ Vcm^{-1} for $X_{DOPG} = 0.40$ is almost similar to $t_{r\_avg} = 34.33 \pm 2.52$ s at $E = 420$ Vcm^{-1} for $X_{DOPG} = 0.10$ and also $t_{r\_avg} = 34.33 \pm 3.79$ s at $E = 470$ Vcm^{-1} for $X_{DOPG} = 0$. These investigations suggest that the mechanical stability of vesicles becomes weaker at higher surface charges in membranes. The electric field dependent P_{rup_60s}, V_c and t_{r_avg} for various X_{DOPG} are presented in Table 2.

3.5 Quantity of electric field for the rupture of GUVs containing various concentrations of cholesterol in their membranes

So far, we investigated how much electric field is required for the rupture of GUVs under various surface charges of membranes. Now the electric field is quantified for the rupture of vesicles containing various concentrations of cholesterol in their membranes. The value of $E = 470$ Vcm^{-1} was applied on a 'single DOPG/DOPC/Chol (46/39/15)-GUV' (here cholesterol mole fraction, Chol = 0.15) for a maximum time 60 s. In this case, the inside of vesicle was 1 mM calcein with 0.10 M sucrose. Prior to apply the pulsed electric field, the inside of GUV shows white color in a fluorescence microscopic image (Fig 6(A)) at 0 s due to this calcein solution.

Table 2. The electric field dependent probability of rupture and average time for various surface charges, cholesterol contents and osmotic pressures (Both X_{DOPG} = 0.60 and Chol = 0 are same membrane. Again, both X_{DOPG} = 0.40 and X_{DOPG} = 0.40 with ΔC^0 = 0 mOsmL^{-1} are same membrane).

Electric field E (Vcm^{-1})	Critical transmembrane voltage, V_c (V)	Membrane composition	Probability of rupture, P_{rup_60s}	Average time of rupture, t_{r_avg} (s)
410	0.77	X_{DOPG} = 0.60	1.0	7.33 ± 1.53
430	0.83	X_{DOPG} = 0.40		6.33 ± 0.58
445	0.84	X_{DOPG} = 0.20		9.47 ± 0.55
455	0.86	X_{DOPG} = 0.10		12.00 ± 3.00
500	0.94	X_{DOPG} = 0		11.67 ± 2.08
410	0.77	Chol = 0	1.0	7.33 ± 1.53
500	0.94	Chol = 0.15		9.33 ± 1.53
575	1.09	Chol = 0.29		12.33 ± 2.08
630	1.17	Chol = 0.40		13.00 ± 1.00
430	0.83	X_{DOPG} = 0.40, ΔC^0 = 0 mOsmL^{-1}	1.0	6.33 ± 0.58
370	0.71	X_{DOPG} = 0.40, ΔC^0 = 13 mOsmL^{-1}		8.67 ± 2.02
300	0.60	X_{DOPG} = 0.40, ΔC^0 = 17 mOsmL^{-1}		10.00 ± 2.65

https://doi.org/10.1371/journal.pone.0262555.t002

During the application of electric field, the spherical shaped GUV starts to rupture at 10.5 s and subsequently a complete rupture occurs at 13 s (Fig 6(A)). The time dependent fluorescence intensity of the same GUV is shown in Fig 6(B). This graph clearly indicates two-stage phenomena; one is intact state of GUV and another is rupture state. Moreover, it gives the exact time of the rupture of GUVs. The abruptly decreasing line of intensity denotes the rupture state. Fig 6(C) shows the dependence of P_{rup_60s} for Chol = 0 (●), 0.15 (■), 0.29 (▼) and 0.40 (⬢) for various E. At a fixed cholesterol mole fraction, the value of P_{rup_60s} increases with the increase of E. However, as the cholesterol increases from 0 to 0.40, the electric field required for the similar P_{rup_60s} value is larger. As an example, P_{rup_60s} = 0.45 ± 0.07 for Chol = 0.15 at E = 435 Vcm^{-1} whereas P_{rup_60s} = 0.48 ± 0.05 for Chol = 0.29 at E = 520 Vcm^{-1}.

Fig 6(D) shows the P_{rup_60s} with various cholesterols for E = 410, 500 and 550 Vcm^{-1}. It is observed that at Chol = 0.15 the value of P_{rup_60s} = 0.20 ± 0.09 is much lower than P_{rup_60s} = 1.0. It means the P_{rup_60s} = 1.0 when E increases from 410 to 500 Vcm^{-1}. Similar tendency is followed for other cholesterol concentrations. These investigations clearly show that as the cholesterol content increases in the membranes of vesicles, the mechanical stability become increases.

We also determine the average time of rupture (t_{r_avg}) for Chol = 0 (●), 0.15 (■), 0.29 (▼) and 0.40 (⬢) for various E (Fig 6(E)). The value of t_{r_avg} decreases with the increases of E for each Chol. As for example, t_{r_avg} = 44.00 ± 2.65 s at E = 410 Vcm^{-1}, t_{r_avg} = 35.00 ± 2.00 s at E = 435 Vcm^{-1}, t_{r_avg} = 22.83 ± 3.82 s at E = 470 Vcm^{-1} and t_{r_avg} = 9.33 ± 1.53 s at E = 500 Vcm^{-1} for Chol = 0.15. The tendency of decreasing the value of t_{r_avg} with electric field for various cholesterol containing membranes is similar. The electric field dependent P_{rup_60s}, V_c and t_{r_avg} for various cholesterol mole fraction are presented in Table 2.

3.6. Quantity of electric field for the rupture of GUVs under various osmotic pressures

The mechanical stability is greatly influenced by the surface charges and the cholesterol content in the membranes of vesicles as observed in sections 3.4 and 3.5. In this section, we quantify the electric field for the rupture of DOPG/DOPC (40/60)-GUVs under different osmotic

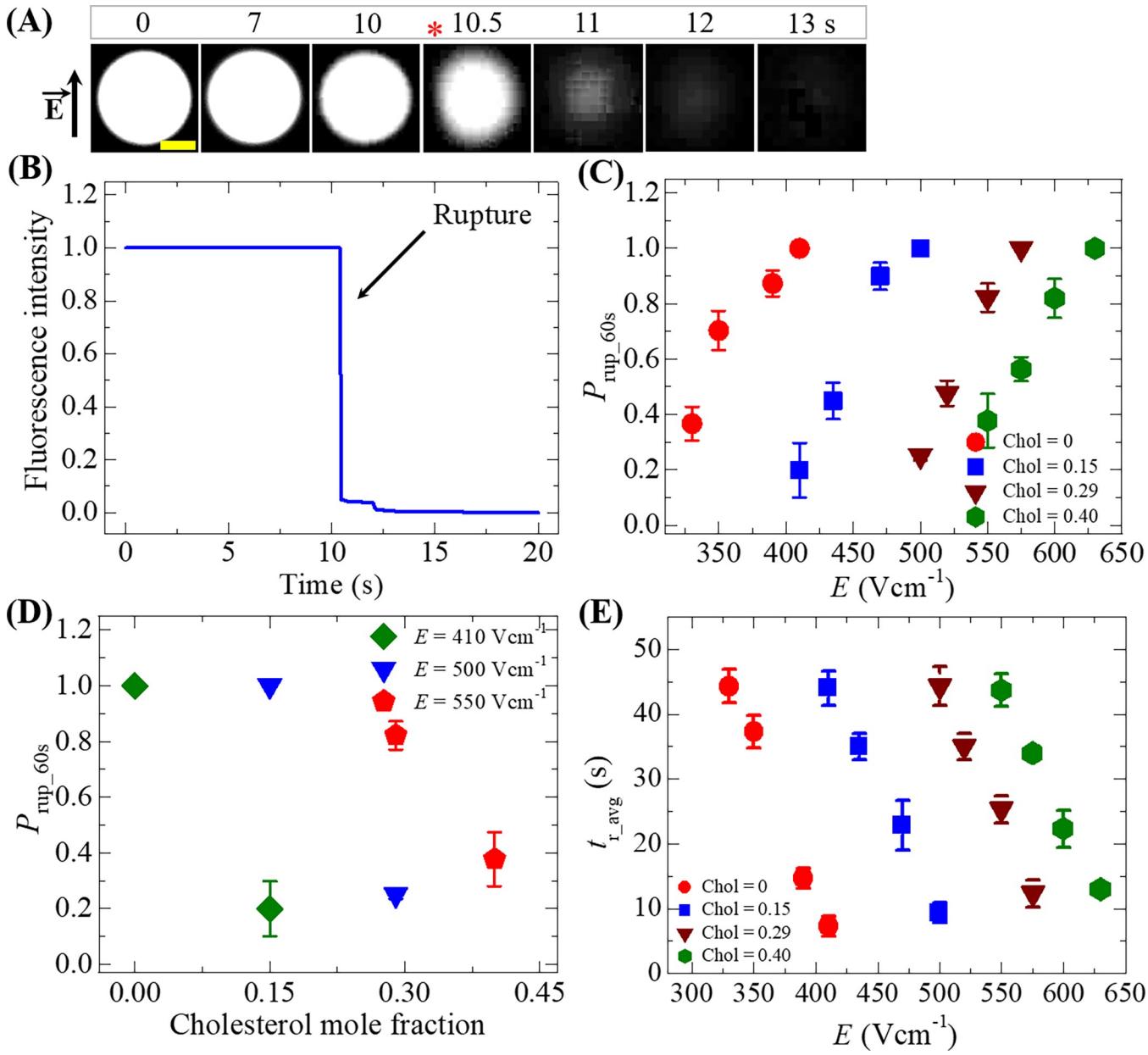

Fig 6. Electric field dependent probability of rupture and the average time of rupture of GUVs containing various cholesterol in their membranes. (A) Fluorescence images of rupture of a 'single DOPG/DOPC/Chol (46/39/15)-GUV' at E = 470 Vcm^{-1}. The field direction is shown with an arrow in the left side of image. The numbers above in each image indicate the time in seconds after applying E. The yellow scale bar is 10 μm. The time of rupture is indicated by asterisk mark (*). (B) The time dependent normalized fluorescence intensity of GUV as shown in (a). (C) The electric field dependent P_{rup_60s} for Chol = 0 (●), 0.15 (■), 0.29 (▼) and 0.40 (⬢). (D) The cholesterol dependent P_{rup_60s} at the values of E = 410 (◆), 500 (▼) and 550 Vcm^{-1} (⬟). (E) The electric field dependent average rupture time, t_{r_avg} for Chol = 0 (●), 0.15 (■), 0.29 (▼) and 0.40 (⬢). Average and standard deviation are calculated from 3 independent experiments using 15–24 GUVs for each case.

https://doi.org/10.1371/journal.pone.0262555.g006

pressures (Π). The osmolarity of the inside sucrose of GUVs,C^0_{in} was 388 mOsmL^{-1}. When GUVs are transferred to a hypotonic solution of concentration C_{out} (mOsmL^{-1}), osmotic pressure is induced in the GUV, which increases the radius of the membrane at swelling equilibrium. The osmolarity difference at an initial condition between the inside and the outside of GUV becomes $\Delta C^0 = C^0_{in} - C_{out}$. We fixed the osmolarity of glucose solution C_{out} = 375 and

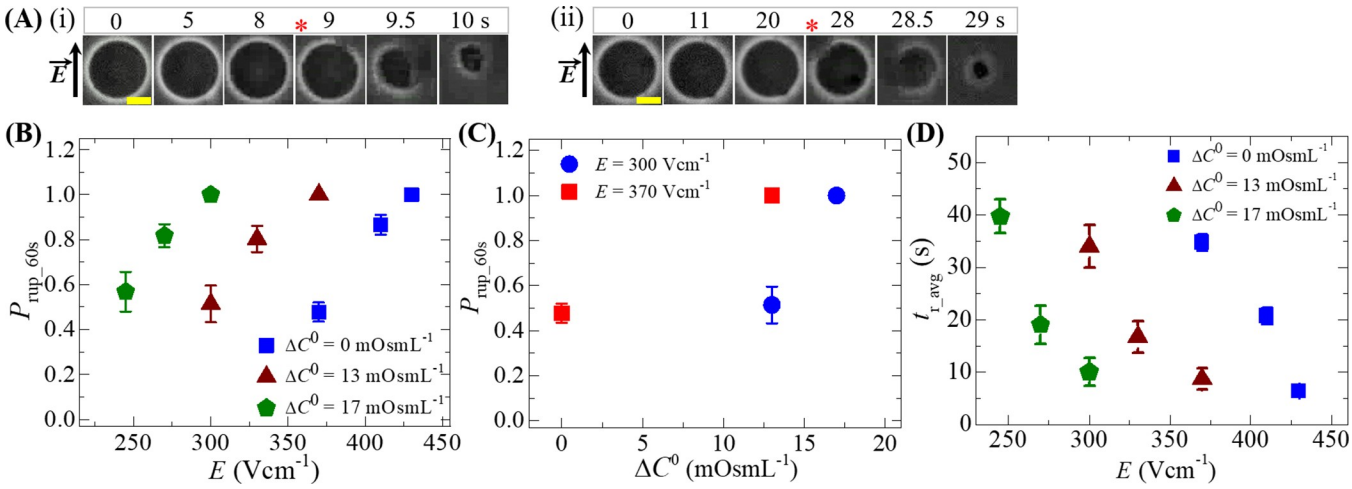

Fig 7. Electric field dependent probability of rupture and the average time of rupture of GUVs in the presence of various osmotic pressures. (A) Phase contrast images of rupture of (i) a 'single DOPG/DOPC (40/60)-GUV' at E = 300 Vcm^{-1} under 17 mOsmL^{-1} and (ii) a 'single DOPG/DOPC (40/60)-GUV' at E = 300 Vcm^{-1} under 13 mOsmL^{-1}. The field direction is shown with an arrow in the left side. The numbers above in each image indicate the time in seconds after application of electric field. The time of rupture is indicated by the asterisk (•). The yellow bar corresponds to a length of 10 μm. (B) The electric field dependent P_{rup_60s} for ΔC^0 = 0 (■), 13 (▲) and 17 mOsmL^{-1} (⬟). (C) The ΔC^0 dependent P_{rup_60s} at E = 370 (■) and 300 Vcm^{-1} (●). (D) The electric field dependent t_{r_avg} for ΔC^0 = 0 (■), 13 (▲) and 17 mOsmL^{-1} (⬟). Average and standard deviation are calculated from 3 independent experiments using 15–24 GUVs in each case.

https://doi.org/10.1371/journal.pone.0262555.g007

371 mOsmL^{-1}, and hence the corresponding ΔC^0 = 13 and 17 mOsmL^{-1}. The detail description of maintaining the osmolarity difference is reported earlier [60]. The phase contrast images of GUV at E = 300 Vcm^{-1} under 17 and 13 mOsmL^{-1} are shown in Fig 7A(i) and 7A(ii), respectively. The corresponding GUVs became rupture at 9 and 28 s. Fig 7(B) shows the electric field dependent P_{rup_60s} for ΔC^0 = 0 (■), 13 (▲) and 17 mOsmL^{-1} (⬟). As the value of ΔC^0 increases, the electric field required for the similar P_{rup_60s} is quite smaller. As an example, P_{rup_60s} = 0.87 ± 0.04 at ΔC^0 = 0 for E = 410 Vcm^{-1} whereas P_{rup_60s} = 0.81 ± 0.06 at ΔC^0 = 13 mOsmL^{-1} for E = 330 Vcm^{-1} and also P_{rup_60s} = 0.82 ± 0.05 at ΔC^0 = 17 mOsmL^{-1} for E = 270 Vcm^{-1}. In all conditions, the value of P_{rup_60s} increases with E. Fig 7(C) shows the P_{rup_60s} for E = 370 (■) and 300 Vcm^{-1} (●) at different ΔC^0. It is found that for E = 300 Vcm^{-1}, P_{rup_60s} = 0.48 ± 0.04 at ΔC^0 = 0 is much lower than P_{rup_60s} = 1.0 at ΔC^0 = 13 mOsmL^{-1}. Besides, P_{rup_60s} = 1.0 can be obtained by decreasing E from 370 to 300 Vcm^{-1} at ΔC^0 = 13 mOsmL^{-1} (Fig 7(C)).

The value of t_{r_avg} for ΔC^0 = 0 (■), 13 (▲) and 17 mOsmL^{-1} (⬟) for various E are shown in Fig 7(D). The t_{r_avg} decreases with the increases of E for each ΔC^0. As for example, t_{r_avg} = 34.00 ± 4.00 s at E = 300 Vcm^{-1}, t_{r_avg} = 16.67 ± 3.06 s at E = 330 Vcm^{-1} and t_{r_avg} = 8.67 ± 2.02 s at E = 370 Vcm^{-1} under ΔC^0 = 13 mOsmL^{-1}. However, the t_{r_avg} = 20.67 ± 1.53 s at E = 410 Vcm^{-1} for ΔC^0 = 0 is similar to the value of t_{r_avg} = 19.00 ± 3.61 s at E = 270 Vcm^{-1} for ΔC^0 = 17 mOsmL^{-1}. These investigations suggest that a lower electric field is required for the rupture of GUVs for higher osmotic pressure. The electric field dependent P_{rup_60s}, V_c and t_{r_avg} for various osmotic pressures are presented in Table 2.

4 Discussion

At first, we performed the COMSOL simulation for estimating the electric field required for the vesicle rupture. Then, we quantify the electric field for different conditions. The rupture of vesicles occurs when the transmembrane voltage is reached to a threshold value (V_c), that is, when the externally applied electric field is above the electroporation threshold value. Electric

field distribution, which is established in lipid membranes when electric current passes through the GUV, is difficult to predict, especially when the targeted vesicle has different conditions. For effective prediction of electric field strength and distribution, we performed the simulation study using the similar experimental condition (Fig 2). The electroporation depends on the effective electric field, which is directly related to the angle between the field and the membrane surface normal. The simulation results also show that the critical electric field strength for vesicle rupture depends linearly on reciprocal of the radius of GUVs, which agrees with Eq (5).

In the experimental study, for getting $P_{rup\_60s} = 1.0$, the value of E changes from 500 to 410 Vcm^{-1} by changing the X_{DOPG} from 0 to 0.60. On the other hand, for getting the same P_{rup_60s}, the value of E changes from 410 to 630 Vcm^{-1} by changing the cholesterol mole fraction from 0 to 0.40. In addition, the value of E changes from 430 to 300 Vcm^{-1} by changing the ΔC^0 from 0 to 17 $mOsmL^{-1}$. A numerical calculation regardless of the vesicle geometry was investigated by applying the electric field 600 Vcm^{-1} in which V_c was 0.80 V [66]. In our simulation, the electric field for rupture of GUV is obtained 350 to 540 Vcm^{-1} at $\theta = 0$, which support that numerical calculation.

The coarse-grained MARTINI force field simulations indicated the instability of lipid membranes at higher electric fields [67]. With the increase of electric field, the undulation amplitude increases and consequently decreases the membrane density, which leads to the formation of pores in the membranes of GUVs. Such pores appear at the highly curved regions of the membranes. The formation of pore reorients the water-bilayer interface. The driving mechanism for the instability of membranes is related to the well-known fact that, when an electric field is applied, the low-energy configuration corresponds to the one where the interface aligns parallel to the applied field [68]. As the higher pulsed electric field creates instability of membranes, the electric field dependent average time for rupture (rupture occurs when the radius of pores increases to infinite within a very short time) of GUVs is lower, that supported our investigations (Fig 3(C)).

The intramembrane electrostatic effect due to the anionic lipids in the membranes destabilize the vesicles [69]. The electrostatic effect became prominent as the anionic charged lipids were added to the membranes [70–72]. Again, as the anionic lipid mole fraction increases in the membranes, the repulsive force between the lipid molecules also increases and hence increases the electrostatic effect [73]. With the increase of electrostatic interaction, the probability of rupture increases and consequently the average time of rupture decreases, supporting our investigation (Fig 5). Hence, membrane electrostatics play vital role for the processes of rupture of lipid vesicles.

Recently, it has been reported that as the cholesterol content increased in the membranes of DOPC vesicles, the bending rigidity increased several folds [59]. The results also indicated the local stiffening in DOPC membranes due to the addition of cholesterol. Buckling simulations on DOPC membranes also indicated the increase of bending rigidity [74]. Therefore, it can be reasonably considered that the membrane instability in cholesterol containing membranes due to electric field became lower compared to the membranes without cholesterol. Therefore, higher electric field is required for the rupture of GUVs as the cholesterol increases in the membranes that follows our investigations (Fig 6).

The electroporation in GUVs under various osmotic pressures was reported earlier [60], where we calculated the membrane tension generated by the osmotic pressures. In present report, we have aimed to quantify the pulsed electric field for the rupture of GUVs with various surface charges, cholesterols and osmotic pressures. It is well reported that the membrane tension due to electric field (σ_e) is connected with transmembrane voltage (V_m) [75,76] by $\sigma_e \propto V_m^2$. Since, $V_m \propto E$, hence $\sigma_e \propto E^2$. Osmotic swelling creates lateral membrane tension (σ_{os})

in the GUVs [77,78]. Therefore, the total tension in the membrane of GUVs is $\sigma_t = \sigma_{os} + \sigma_e$ (if there is no osmotic effect, $\sigma_t = \sigma_e$). With the increase of osmotic pressure, the value of σ_t increases, and therefore, the stability of membranes decreases. Again, the probability of rupture is defined as follows [79]:

$$P_{rup\_t} = 1 - \exp(-k_p t_{EF}) \tag{7}$$

where, k_p is the rate constant of vesicle rupture. Generally, the rate constant for any reaction can be expressed by the following well-known Arrhenius equation [80]:

$$k_p = A\exp(-U_b/k_B T) \tag{8}$$

where, A is a constant whose unit is s^{-1}, k_B is the Boltzmann constant and T is the absolute temperature. According to the classical theory of pore formation in lipid bilayers, the energy barrier of a prepore at a critical radius is defined as follows [79,81]:

$$U_b(r, \sigma_t) = \frac{\pi\Gamma^2}{\sigma_t + B} \tag{9}$$

where, B is the electrostatic term for charged lipids in membranes [72], Γ is the line tension of a prepore and r is the prepore radius.

As the anionic lipid in membranes increases, the repulsive force between the anionic lipids becomes stronger. Such stronger effect increases the value of B and decreases the value of U_b (see Eq 9), which ultimately increases the probability of rupture (using Eqs 7 and 8) as obtained in Fig 5. Again, several reports indicated that the increase of cholesterol increase the value of Γ [82–85]. The higher is the value of Γ, the lower the value of U_b, which eventually decreases the probability of rupture as found in Fig 6. Lastly, with the increase of osmotic gradient, the value of σ_{os} in σ_t increases. With the increased σ_{os}, the value of U_b decreases, and consequently increases the rupture probability. This explanation is consistent with the result mentioned in Fig 7. Therefore, the above discussion supports our investigations.

5 Conclusions

We quantify the pulsed electric field required for the rupture of GUVs along with the behavior of such vesicles exposed to electric field. The optically detectable rupture is identified in the phase contrast and fluorescence images due to the disruption in membrane integrity. The amount of electric field required for vesicle rupture depends on the surface charges, cholesterol contents and the osmotic pressures. Addition of anionic lipid in membranes requires relatively lower electric field for the rupture of GUVs. In contrast, higher cholesterol content requires relatively higher electric field for vesicle rupture. Again, the value of applied electric field for vesicle rupture is greatly influenced by the osmotic gradient, indicating that higher gradient required lower electric field. Such differences are well explained by the mechanical stability of membranes of vesicles. The pore formation in the membranes of vesicles and consequently the rupture of vesicles are explained by the well accepted classical theory of pore formation in lipid bilayers. These investigations provide quantitative and valuable information on the electric field dependent rupture of GUVs under various conditions. This study serves as a guideline for further experiments in this area and offers an entrancing biophysical description of the phenomenon of electroporation in vesicles together with the insight of biological consequences.

Author Contributions

Conceptualization: Md. Kabir Ahamed, Marzuk Ahmed, Mohammad Abu Sayem Karal.

Data curation: Md. Kabir Ahamed, Marzuk Ahmed, Mohammad Abu Sayem Karal.

Formal analysis: Md. Kabir Ahamed, Marzuk Ahmed, Mohammad Abu Sayem Karal.

Funding acquisition: Mohammad Abu Sayem Karal.

Investigation: Md. Kabir Ahamed, Marzuk Ahmed, Mohammad Abu Sayem Karal.

Methodology: Md. Kabir Ahamed, Marzuk Ahmed, Mohammad Abu Sayem Karal.

Project administration: Mohammad Abu Sayem Karal.

Resources: Mohammad Abu Sayem Karal.

Supervision: Mohammad Abu Sayem Karal.

Validation: Md. Kabir Ahamed, Marzuk Ahmed, Mohammad Abu Sayem Karal.

Visualization: Mohammad Abu Sayem Karal.

Writing – original draft: Md. Kabir Ahamed, Marzuk Ahmed, Mohammad Abu Sayem Karal.

Writing – review & editing: Md. Kabir Ahamed, Marzuk Ahmed, Mohammad Abu Sayem Karal.

References

1. Maton A. Cells: building blocks of life. Upper Saddle River, N.J.: Prentice-Hall; 1997.
2. Iwasa J, Marshall WF, Karp Gerald. Karp's cell and molecular biology: concepts and experiments. 8th ed., John Wiley & Sons, 2016.
3. Fricke H, Morse S. The electric resistance and capacity of blood for frequencies between 800 and 4½ million cycles. J Gen Physiol. 1925; 9: 153–167. https://doi.org/10.1085/jgp.9.2.153 PMID: 19872239
4. Cole KS, Baker RF. Longitudinal impedance of the squid giant axon. J Gen Physiol. 1941; 24: 771–788. https://doi.org/10.1085/jgp.24.6.771 PMID: 19873252
5. Raicu V, Feldman Y, editors. Dielectric relaxation in biological systems: physical principles, methods, and applications. Oxford: Oxford University Press; 2015. https://doi.org/10.1093/acprof:oso/9780199686513.001.0001
6. Brown BH, Smallwood RH, Barber DC, Lawford PV, Hose DR. Medical Physics and Biomedical Engineering. 1st ed. Bristol; Philadelphia: CRC Press; 1998. PMID: 9616990
7. Claret B, Claret M, Mazet JL. Ionic transport and membrane potential of rat liver cells in normal and low-chloride solutions. J Physiol. 1973; 230: 87–101. https://doi.org/10.1113/jphysiol.1973.sp010176 PMID: 4702455
8. Yang M, Brackenbury W. Membrane potential and cancer progression. Front Physiol. 2013; 4: 185. https://doi.org/10.3389/fphys.2013.00185 PMID: 23882223
9. Weaver JC, Chizmadzhev YuA. Theory of electroporation: A review. Bioelectrochem Bioenerg. 1996; 41: 135–160. https://doi.org/10.1016/S0302-4598(96)05062-3
10. Mir LM, Devauchelle P, Quintin-Colonna F, Delisle F, Doliger S, Fradelizi D, et al. First clinical trial of cat soft-tissue sarcomas treatment by electrochemotherapy. Br J Cancer. 1997; 76: 1617–1622. https://doi.org/10.1038/bjc.1997.606 PMID: 9413951
11. Teissie J, Golzio M, Rols MP. Mechanisms of cell membrane electropermeabilization: A minireview of our present (lack of?) knowledge. Biochim Biophys Acta (BBA)—General Subjects. 2005; 1724: 270–280. https://doi.org/10.1016/j.bbagen.2005.05.006 PMID: 15951114
12. Cheng H-T, Megha, London E. Preparation and properties of asymmetric vesicles that mimic cell membranes. J Biol Chem. 2009; 284: 6079–6092. https://doi.org/10.1074/jbc.M806077200 PMID: 19129198
13. Walde P, Cosentino K, Engel H, Stano P. Giant vesicles: preparations and applications. ChemBioChem. 2010; 11: 848–865. https://doi.org/10.1002/cbic.201000010 PMID: 20336703

14. Ivorra A, Villemejane J, Mir LM. Electrical modeling of the influence of medium conductivity on electroporation. Phys Chem Chem Phys. 2010; 12: 10055–10064. https://doi.org/10.1039/c004419a PMID: 20585676

15. Silve A, Leray I, Poignard C, Mir LM. Impact of external medium conductivity on cell membrane electropermeabilization by microsecond and nanosecond electric pulses. Sci Rep. 2016; 6: 19957. https://doi.org/10.1038/srep19957 PMID: 26829153

16. Freeman SA, Wang MA, Weaver JC. Theory of electroporation of planar bilayer membranes: predictions of the aqueous area, change in capacitance, and pore-pore separation. Biophys J. 1994; 67: 42–56. https://doi.org/10.1016/S0006-3495(94)80453-9 PMID: 7919016

17. Heimburg T. The capacitance and electromechanical coupling of lipid membranes close to transitions: the effect of electrostriction. Biophys J. 2012; 103: 918–929. https://doi.org/10.1016/j.bpj.2012.07.010 PMID: 23009841

18. Frey W, White JA, Price RO, Blackmore PF, Joshi RP, Nuccitelli R, et al. Plasma membrane voltage changes during nanosecond pulsed electric field exposure. Biophys J. 2006; 90: 3608–3615. https://doi.org/10.1529/biophysj.105.072777 PMID: 16513782

19. Teissie J. Critical electric field and transmembrane voltage for lipid pore formation in experiments. In: Miklavcic D, editor. Handbook of electroporation. Cham: Springer International Publishing; 2017. pp. 1–19. https://doi.org/10.1007/978-3-319-26779-1_77–1

20. Sandre O, Moreaux L, Brochard-Wyart F. Dynamics of transient pores in stretched vesicles. PNAS. 1999; 96: 10591–10596. https://doi.org/10.1073/pnas.96.19.10591 PMID: 10485870

21. Portet T, Mauroy C, Démery V, Houles T, Escoffre J-M, Dean DS, et al. Destabilizing giant vesicles with electric fields: an overview of current applications. J Membrane Biol. 2012; 245: 555–564. https://doi.org/10.1007/s00232-012-9467-x PMID: 22864479

22. Karal MAS, Ahamed MK, Rahman M, Ahmed M, Shakil MM, Rabbani KS. Effects of electrically-induced constant tension on giant unilamellar vesicles using irreversible electroporation. Eur Biophys J. 2019; 48: 731–741. https://doi.org/10.1007/s00249-019-01398-9 PMID: 31552440

23. Jordan CA, Neumann E, Sowers AE, editors. Electroporation and Electrofusion in Cell Biology. Springer US; 1989. https://doi.org/10.1007/978-1-4899-2528-2

24. Raz-Ben Aroush D, Yehudai-Resheff S, Keren K. Chapter 22—Electrofusion of giant unilamellar vesicles to cells. In: Paluch EK, editor. Methods in Cell Biology. Academic Press; 2015. pp. 409–422. https://doi.org/10.1016/bs.mcb.2014.11.005 PMID: 25640441

25. Zimmermann U, Neil GA. Electromanipulation of cells. Boca Raton, Fla.: CRC Press; 1996.

26. Riske KA, Dimova R. Electro-deformation and poration of giant vesicles viewed with high temporal resolution. Biophys J. 2005; 88: 1143–1155. https://doi.org/10.1529/biophysj.104.050310 PMID: 15596488

27. Riske KA, Dimova R. Electric pulses induce cylindrical deformations on giant vesicles in salt solutions. Biophys J. 2006; 91: 1778–1786. https://doi.org/10.1529/biophysj.106.081620 PMID: 16766621

28. Ambjörnsson T, Lomholt MA, Hansen PL. Applying a potential across a biomembrane: Electrostatic contribution to the bending rigidity and membrane instability. Phys Rev E. 2007; 75: 051916. https://doi.org/10.1103/PhysRevE.75.051916 PMID: 17677107

29. Hu Q, Zhang Z, Qiu H, Kong MG, Joshi RP. Physics of nanoporation and water entry driven by a high-intensity, ultrashort electrical pulse in the presence of membrane hydrophobic interactions. Phys Rev E. 2013; 87: 032704. https://doi.org/10.1103/PhysRevE.87.032704

30. Gowrishankar TR, Weaver JC. An approach to electrical modeling of single and multiple cells. PNAS. 2003; 100: 3203–3208. https://doi.org/10.1073/pnas.0636434100 PMID: 12626744

31. Zimmermann U. Electrical breakdown, electropermeabilization and electrofusion. Reviews of Physiology, Biochemistry and Pharmacology, Volume 105. Berlin, Heidelberg: Springer Berlin Heidelberg; 1986. pp. 175–256. https://doi.org/10.1007/BFb0034499

32. Usaj M, Kanduser M. The systematic study of the electroporation and electrofusion of B16-F1 and CHO cells in isotonic and hypotonic buffer. J Membrane Biol. 2012; 245: 583–590. https://doi.org/10.1007/s00232-012-9470-2 PMID: 22843161

33. Mir LM. Bases and rationale of the electrochemotherapy. Eur J Cancer Suppl. 2006; 4: 38–44. https://doi.org/10.1016/j.ejcsup.2006.08.005

34. Sersa G, Miklavcic D, Cemazar M, Rudolf Z, Pucihar G, Snoj M. Electrochemotherapy in treatment of tumours. Eur J Surg Oncol. 2008; 34: 232–240. https://doi.org/10.1016/j.ejso.2007.05.016 PMID: 17614247

35. Golzio M, Rols MP, Teissié J. In vitro and in vivo electric field-mediated permeabilization, gene transfer, and expression. Methods. 2004; 33: 126–135. https://doi.org/10.1016/j.ymeth.2003.11.003 PMID: 15121167

36. Cemazar M, Jarm T, Sersa G. Cancer electrogene therapy with interleukin-12. Curr Gene Ther. 2010; 10: 300–311. https://doi.org/10.2174/156652310791823425 PMID: 20560875

37. Rubinsky B. Irreversible electroporation in medicine. Technol Cancer Res Treat. 2007; 6: 255–259. https://doi.org/10.1177/153033460700600401 PMID: 17668932

38. Gothelf A, Mir LM, Gehl J. Electrochemotherapy: results of cancer treatment using enhanced delivery of bleomycin by electroporation. Cancer Treat Rev. 2003; 29: 371–387. https://doi.org/10.1016/s0305-7372(03)00073-2 PMID: 12972356

39. Schoenbach KH, Hargrave SJ, Joshi RP, Kolb JF, Nuccitelli R, Osgood C, et al. Bioelectric effects of intense nanosecond pulses. IEEE Transactions on Dielectrics and Electrical Insulation. 2007; 14: 1088–1109. https://doi.org/10.1109/TDEI.2007.4339468

40. Mahnič-Kalamiza S, Vorobiev E, Miklavčič D. Electroporation in food processing and biorefinery. J Membrane Biol. 2014; 247: 1279–1304. https://doi.org/10.1007/s00232-014-9737-x PMID: 25287023

41. Aronsson K, Rönner U, Borch E. Inactivation of Escherichia coli, Listeria innocua and Saccharomyces cerevisiae in relation to membrane permeabilization and subsequent leakage of intracellular compounds due to pulsed electric field processing. International J Food Microb. 2005; 99: 19–32. https://doi.org/10.1016/j.ijfoodmicro.2004.07.012 PMID: 15718026

42. Zhao W, Yang R, Liang Q, Zhang W, Hua X, Tang Y. Electrochemical reaction and oxidation of lecithin under pulsed electric fields (PEF) processing. J Agric Food Chem. 2012; 60: 12204–12209. https://doi.org/10.1021/jf304236h PMID: 23185993

43. Ahamed MK, Karal MAS, Ahmed M, Ahammed S. Kinetics of irreversible pore formation under constant electrical tension in giant unilamellar vesicles. Eur Biophys J. 2020; 49: 371–381. https://doi.org/10.1007/s00249-020-01440-1 PMID: 32494845

44. Sens P, Isambert H. Undulation instability of lipid membranes under an electric field. Phys Rev Lett. 2002; 88: 128102. https://doi.org/10.1103/PhysRevLett.88.128102 PMID: 11909504

45. Staykova M, Lipowsky R, Dimova R. Membrane flow patterns in multicomponent giant vesicles induced by alternating electric fields. Soft Matter. 2008; 4: 2168–2171. https://doi.org/10.1039/b811876k PMID: 22096459

46. Weaver JC, Smith KC, Esser AT, Son RS, Gowrishankar TR. A brief overview of electroporation pulse strength–duration space: A region where additional intracellular effects are expected. Bioelectrochem. 2012; 87: 236–243. https://doi.org/10.1016/j.bioelechem.2012.02.007 PMID: 22475953

47. Uitert I van Gac SL, Berg A van den. Determination of the electroporation onset of bilayer lipid membranes as a novel approach to establish ternary phase diagrams: example of the L-α-PC/SM/cholesterol system. Soft Matter. 2010; 6: 4420–4429. https://doi.org/10.1039/C0SM00181C

48. Delemotte L, Klein M, Tarek M. Molecular dynamics simulations of voltage-gated cation channels: insights on voltage-sensor domain function and modulation. Front Pharmacol. 2012; 3: 97. https://doi.org/10.3389/fphar.2012.00097 PMID: 22654756

49. Rems L. Chapter One—Applicative use of electroporation models: from the molecular to the tissue level. In: Iglič A, Rappolt M, García-Sáez AJ, editors. Advances in biomembranes and lipid self-assembly. Academic Press; 2017. pp. 1–50. https://doi.org/10.1016/bs.abl.2017.06.001

50. Kotnik T, Rems L, Tarek M, Miklavčič D. Membrane electroporation and electropermeabilization: mechanisms and models. Annu Rev Biophys. 2019; 48: 63–91. https://doi.org/10.1146/annurev-biophys-052118-115451 PMID: 30786231

51. Reeves JP, Dowben RM. Formation and properties of thin-walled phospholipid vesicles. J Cell Physiol. 1969; 73: 49–60. https://doi.org/10.1002/jcp.1040730108 PMID: 5765779

52. Tamba Y, Terashima H, Yamazaki M. A membrane filtering method for the purification of giant unilamellar vesicles. Chem Phys Lipids. 2011; 164: 351–358. https://doi.org/10.1016/j.chemphyslip.2011.04.003 PMID: 21524642

53. Karal MAS, Rahman M, Ahamed MK, Shibly SUA, Ahmed M, Shakil MM. Low cost non-electromechanical technique for the purification of giant unilamellar vesicles. Eur Biophys J. 2019; 48: 349–359. https://doi.org/10.1007/s00249-019-01363-6 PMID: 30918998

54. Nagle JF, Tristram-Nagle S. Structure of lipid bilayers. Biochim Biophys Acta (BBA)—Rev Biomembr. 2000; 1469: 159–195. https://doi.org/10.1016/S0304-4157(00)00016-2

55. de Meyer F, Smit B. Effect of cholesterol on the structure of a phospholipid bilayer. PNAS. 2009; 106: 3654–3658. https://doi.org/10.1073/pnas.0809959106 PMID: 19225105

56. Alwarawrah M, Dai J, Huang J. A Molecular view of the cholesterol condensing effect in DOPC lipid bilayers. J Phys Chem B. 2010; 114: 7516–7523. https://doi.org/10.1021/jp101415g PMID: 20469902

57. Armstrong CL, Marquardt D, Dies H, Kučerka N, Yamani Z, Harroun TA, et al. The observation of highly ordered domains in membranes with cholesterol. PLOS ONE. 2013; 8: e66162. https://doi.org/10.1371/journal.pone.0066162 PMID: 23823623

58. Magarkar A, Dhawan V, Kallinteri P, Viitala T, Elmowafy M, Róg T, et al. Cholesterol level affects surface charge of lipid membranes in saline solution. Sci Rep. 2014; 4: 1–5. https://doi.org/10.1038/srep05005 PMID: 24845659

59. Chakraborty S, Doktorova M, Molugu TR, Heberle FA, Scott HL, Dzikovski B, et al. How cholesterol stiffens unsaturated lipid membranes. PNAS. 2020; 117: 21896–21905. https://doi.org/10.1073/pnas.2004807117 PMID: 32843347

60. Sarkar MK, Karal MAS, Ahmed M, Ahamed MK, Ahammed S, Sharmin S, et al. Effects of osmotic pressure on the irreversible electroporation in giant lipid vesicles. PLOS ONE. 2021; 16: e0251690. https://doi.org/10.1371/journal.pone.0251690 PMID: 33989363

61. Datta AK, Rakesh V. An introduction to modeling of transport processes: applications to biomedical systems. Cambridge, UK; New York: Cambridge University Press; 2010.

62. Langus J, Kranjc M, Kos B, Šuštar T, Miklavčič D. Dynamic finite-element model for efficient modelling of electric currents in electroporated tissue. Sci Rep. 2016; 6: 26409. https://doi.org/10.1038/srep26409 PMID: 27211822

63. Karal MAS, Ahamed MK, Ahmed M. Development of an irreversible electroporation (IRE) device for vesicle ablation. 2020 11th International Conference on Electrical and Computer Engineering (ICECE). 2020. pp. 318–321. https://doi.org/10.1109/ICECE51571.2020.9393089

64. Grosse C, Schwan HP. Cellular membrane potentials induced by alternating fields. Biophys J. 1992; 63: 1632–1642. https://doi.org/10.1016/S0006-3495(92)81740-X PMID: 19431866

65. Karal MAS, Levadnyy V, Yamazaki M. Analysis of constant tension-induced rupture of lipid membranes using activation energy. Phys Chem Chem Phys. 2016; 18: 13487–13495. https://doi.org/10.1039/c6cp01184e PMID: 27125194

66. Muralidharan A, Rems L, Kreutzer MT, Boukany PE. Actin networks regulate the cell membrane permeability during electroporation. Biochim Biophys Acta (BBA)—Biomembr. 2021; 1863: 183468. https://doi.org/10.1016/j.bbamem.2020.183468 PMID: 32882211

67. Prathyusha KR, Pagonabarraga I, Kumar PBS. Modification of lipid membrane compressibility induced by an electric field. Phys Rev E. 2020; 102: 062413. https://doi.org/10.1103/PhysRevE.102.062413 PMID: 33466026

68. Tsori Y. Colloquium: Phase transitions in polymers and liquids in electric fields. Rev Mod Phys. 2009; 81: 1471–1494. https://doi.org/10.1103/RevModPhys.81.1471

69. Shoemaker SD, Vanderlick TK. Intramembrane electrostatic interactions destabilize lipid vesicles. Biophys J. 2002; 83: 2007–2014. https://doi.org/10.1016/S0006-3495(02)73962-3 PMID: 12324419

70. Cevc G. Membrane electrostatics. Biochim Biophys Acta (BBA)—Rev Biomembr. 1990; 1031: 311–382. https://doi.org/10.1016/0304-4157(90)90015-5 PMID: 2223819

71. Betterton MD, Brenner MP. Electrostatic edge instability of lipid membranes. Phys Rev Lett. 1999; 82: 1598–1601. https://doi.org/10.1103/PhysRevLett.82.1598

72. Karal M, Levadnyy V, Tsuboi T-A, Belaya M, Yamazaki M. Electrostatic interaction effects on tension-induced pore formation in lipid membranes. Phys Rev E. 2015; 92: 012708. https://doi.org/10.1103/PhysRevE.92.012708 PMID: 26274204

73. Israelachvili JN. Intermolecular and surface forces. Elsevier; 2011. pp. 291–340. https://doi.org/10.1016/B978-0-12-375182-9.10014–4

74. Eid J, Razmazma H, Jraij A, Ebrahimi A, Monticelli L. On calculating the bending modulus of lipid bilayer membranes from buckling simulations. J Phys Chem B. 2020; 124: 6299–6311. https://doi.org/10.1021/acs.jpcb.0c04253 PMID: 32597189

75. Dimova R, Bezlyepkina N, Jordö MD, Knorr RL, Riske KA, Staykova M, et al. Vesicles in electric fields: Some novel aspects of membrane behavior. Soft Matter. 2009; 5: 3201. https://doi.org/10.1039/b901963d

76. Abidor IG, Arakelyan VB, Chernomordik LV, Chizmadzhev YuA, Pastushenko VF, Tarasevich MP. Electric breakdown of bilayer lipid membranes: I. The main experimental facts and their qualitative discussion. J Electroanal Chem Interf Electrochem. 1979; 104: 37–52. https://doi.org/10.1016/S0022-0728(79)81006-2

77. Shibly SUA, Ghatak C, Karal MAS, Moniruzzaman M, Yamazaki M. Experimental estimation of membrane tension induced by osmotic pressure. Biophys J. 2016; 111: 2190–2201. https://doi.org/10.1016/j.bpj.2016.09.043 PMID: 27851942

78. Saha SK, Shibly SUA, Yamazaki M. Membrane tension in negatively charged lipid bilayers in a buffer under osmotic pressure. J Phys Chem B. 2020; 124: 5588–5599. https://doi.org/10.1021/acs.jpcb.0c03681 PMID: 32543195

79. Levadny V, Tsuboi T, Belaya M, Yamazaki M. Rate constant of tension-induced pore formation in lipid membranes. Langmuir. 2013; 29: 3848–3852. https://doi.org/10.1021/la304662p PMID: 23472875

80. Laidler KJ. Chemical kinetics. New York: Harper & Row; 1987. https://doi.org/10.1016/s0076-6879(87)36008-2 PMID: 3683196

81. Litster JD. Stability of lipid bilayers and red blood cell membranes. Phys Lett A. 1975; 53: 193–194. https://doi.org/10.1016/0375-9601(75)90402-8

82. Needham D, Hochmuth RM. Electro-mechanical permeabilization of lipid vesicles. Role of membrane tension and compressibility. Biophys J. 1989; 55: 1001–1009. https://doi.org/10.1016/S0006-3495(89)82898-X PMID: 2720075

83. Zhelev DV, Needham D. Tension-stabilized pores in giant vesicles: determination of pore size and pore line tension. Biochim Biophys Acta. 1993; 1147: 89–104. https://doi.org/10.1016/0005-2736(93)90319-u PMID: 8466935

84. Karatekin E, Sandre O, Guitouni H, Borghi N, Puech P-H, Brochard-Wyart F. Cascades of transient pores in giant vesicles: line tension and transport. Biophys J. 2003; 84: 1734–1749. https://doi.org/10.1016/S0006-3495(03)74981-9 PMID: 12609875

85. Portet T, Dimova R. A new method for measuring edge tensions and stability of lipid bilayers: effect of membrane composition. Biophys J. 2010; 99: 3264–3273. https://doi.org/10.1016/j.bpj.2010.09.032 PMID: 21081074